Room-temperature ferromagnetism and anomalous Hall effect in $Si_{1-x}Mn_x$ ($x \approx 0.35$) alloys

B. A. Aronzon,[1,8,*] V. V. Rylkov,[1,9,†] S. N. Nikolaev,[1] V. V. Tugushev,[1,‡] S. Caprara,[2,§] V. V. Podolskii,[3] V. P. Lesnikov,[3] A. Lashkul,[4] R. Laiho,[5] R. R. Gareev,[6] N. S. Perov,[7] and A. S. Semisalova[7]

[1]*Russian Research Centre "Kurchatov Institute," Moscow 123182, Russia*
[2]*Dipartimento di Fisica, Università di Roma "La Sapienza," piazzale Aldo Moro 2, I-00185 Roma, Italy*
[3]*Physicotechnical Research Institute, Nizhnii Novgorod State University, Nizhnii Novgorod 603950, Russia*
[4]*Lappeenranta University of Technology, Lappeenranta, P.O. Box 20, FIN-53850 Finland*
[5]*Wihuri Physical Laboratory, Turku University, Turku FIN-20014, Finland*
[6]*Institute of Experimental and Applied Physics, University of Regensburg, D-93040 Regensburg, Germany*
[7]*Faculty of Physics, M.V. Lomonosov MSU, Moscow 119992, Russia*
[8]*Institute of Applied and Theoretical Electrodynamics, Russian Academy of Sciences, Moscow 127412, Russia*
[9]*Kotel'nikov Institute of Radio Engineering and Electronics, Russian Academy of Sciences, Fryazino, Moscow District 141190, Russia*

(Received 6 December 2010; revised manuscript received 24 June 2011; published 12 August 2011)

A detailed study of the magnetic and transport properties of $Si_{1-x}Mn_x$ ($x \approx 0.35$) films is presented. We observe the anomalous Hall effect in these films up to room temperature. The results of the magnetic measurements and the anomalous Hall effect data are consistent and demonstrate the existence of long-range ferromagnetic order in the systems under investigation. A correlation of the anomalous Hall effect and the magnetic properties of the samples with their conductivity and substrate type is shown. A theoretical model based on the idea of a two-phase magnetic material, in which molecular clusters with localized magnetic moments are embedded in the matrix of a weak itinerant ferromagnet, is discussed and used to explain experimental results. The long-range ferromagnetic order at high temperatures is mainly due to the Stoner enhancement of the exchange coupling between clusters through thermal spin fluctuations ("paramagnons") in the matrix. Theoretical predictions do not contradict experimental data when model parameters of a plausible order of magnitude are used.

DOI: 10.1103/PhysRevB.84.075209 PACS number(s): 72.25.Dc, 75.47.−m, 75.50.Pp

I. INTRODUCTION

Materials which display both high-temperature ferromagnetism and good semiconducting properties are of great interest for basic research and respond to the challenging search for electronics applications in which both the charge and the spin of the electrons are used for information storage and processing.[1] Materials that consist of magnetic transition metals embedded in a nonmagnetic semiconductor, hereafter referred to as the matrix, are the most promising for this purpose. It is widely accepted that such materials could be used for injection of spin-polarized carriers into a normal semiconductor at temperatures above room temperature.[1] Up to now the related studies were mainly oriented toward dilute magnetic semiconductors (DMSs) based on Mn-doped III-V semiconducting materials (III-Mn-V, mostly GaMnAs). In such materials, if the Mn concentration is not too high, Mn substitutes for Ga, acting as an acceptor, so doping GaAs with Mn yields both local magnetic moments and free holes.[2,3] Ferromagnetic (FM) ordering in this case is due to an indirect exchange between Mn atoms accompanied by the spin polarization of holes which may reach 80%.[4,5] On the other hand, there are few papers dealing with FM ordering in Mn-doped Si, in spite of the fact that such structures are mostly interesting, due to the compatibility with mainstream silicon technology.

It is known[6] that isolated Mn impurities occupy mainly tetrahedral interstitial positions (Mn_T^-, Mn_T^0, Mn_T^+, Mn_T^{2+}) in the Si lattice acting as donors,[2,3] while a strong hybridization of Mn $3d$ states with $4(s,p)$ states in Si and an indirect exchange between Mn moments appears if they enter into substitutional positions (Mn_{Si}^{2-}, Mn_{Si}^+) as acceptors.[2,7] The combined simultaneous deposition of Mn and Si may lead to the formation of manganese silicide Mn_nSi_m films, with the ratio (m/n) ranging between 1.70 and 1.75 (for example, Mn_4Si_7, $Mn_{11}Si_{19}$, $Mn_{15}Si_{26}$, $Mn_{26}Si_{45}$, $Mn_{27}Si_{47}$).[8] These phases may exhibit semiconducting, metallic, or half-metallic behavior.[9] For example, ideally stoichiometric and unstressed Mn_4Si_7 is shown to be a semiconductor with an indirect band gap, although a small nonstoichiometry or lattice stress leads to the closure of the gap, turning the semiconductor into a semimetal or a metal. It is important to notice that some manganese silicides[8–10] are weak itinerant ferromagnets with Curie temperatures $T_C < 50$ K. It should also be noted that electron transport in Mn_nSi_m films is not well known, and to our knowledge the resistivity and Hall effect in Mn_4Si_7 have been studied only in Ref. 8.

Si-based DMSs attracted interest after the observation of a FM state with high Curie temperature $T_C > 400$ K, in these materials.[11] This result was obtained in Si:Mn films with a relatively low (0.1–0.8 at.%) content of implanted Mn ions, but its origin remained mysterious. Since a FM state was also observed in Si after implantation of nonmagnetic ions (Ar,Si) or irradiated by neutrons, some authors argued that high-temperature ferromagnetism in Si-based DMSs is due to paramagnetic defects.[12,13]

Detailed x-ray and magnetic studies of Mn-implanted Si indicated that the Mn ions not only enter in the substitutional or interstitial positions of the Si lattice, but also form molecular clusters.[13–15] It may then be assumed[16] that the FM signal is due to such clusters arising during the growth process. Thus, Si-based DMSs seem to be very inhomogeneous alloys and their magnetic properties strongly differ from those of bulk

Mn_nSi_m materials. Furthermore, the formation of the bulk Mn_nSi_m precipitate particles in these DMSs may not be itself the reason for FM ordering, because, as we remarked above, the Mn_nSi_m silicides have a Curie temperature $T_C < 50$ K. It should also be mentioned that the effective magnetic moment per Mn atom ($>0.2\ \mu_B$/Mn) in Mn-implanted Si (Refs. 15 and 18) is quite large as compared with that in bulk Mn_nSi_m [for example, $\approx 0.012\ \mu_B$/Mn in Mn_4Si_7 (Ref. 8)].

Recently, it was calculated[17] that stable FM angstrom-sized Mn-Si complexes can appear in the Si matrix; they contain two or three Mn atoms (dimers or trimers) and have effective magnetic moments $(2–3)\mu_B$/Mn. In $Si_{1-x}Mn_x$ alloys, such complexes can also be self-organized in isolated nanometer-sized ($\approx$20 nm) $Si_{1-x}Mn_x$ ($x \approx 0.35$) precipitate grains containing some hundreds or even thousands of Mn atoms.[15] So, in samples with a relatively low Mn content, the FM signal is probably not due to the formation of a global FM state of isolated Mn moments coupled via spin-polarized carriers, but could be rather attributed to isolated FM angstrom-sized complexes or nanometer-sized precipitate grains. As a result, Si:Mn systems with low Mn content attract less interest for spintronics and the main trend of research is devoted to materials with a relatively high Mn content. However, for these materials the situation is also controversial. For example, a FM state with $T_C \approx 250$ K was observed in uniformly doped $Si_{1-x}Mn_x$ ($x = 0.03–0.05$) films prepared by magnetron sputtering followed with fast annealing.[19] High T_C values ($\approx$300 K) were also recently observed in digital heterostructures with alternating deposition of Mn and Si thin layers with average Mn content 5–10 at.%.[20] On the other hand, amorphous $Si_{1-x}Mn_x$ films with $x = (0.005–0.175)$, obtained by a similar method, showed extremely small magnetic moments per Mn atom and the Curie temperature did not exceed 2 K.[21]

Thus, we can conclude that the mechanism for FM ordering at $T > 50$ K in Si doped with Mn is far from understood. Furthermore, the results obtained for samples prepared by similar techniques could contradict one another (compare, for example, the results published in Refs. 11 and 15 or in Refs. 20 and 21).

The common feature of the main experimental results[11–13,15,16,18–21] is that they were based on magnetization measurements, which cannot provide the proof of global FM order and spin polarization of the carriers. For example, the hysteresis loop of magnetization can be observed even at room temperature in III-Mn-V DMSs with embedded FM nanograins (MnAs or MnSb), while the anomalous contribution to the Hall effect related to the carrier spin polarization is absent (see Ref. 22 and references therein). To get at least a hint of the carrier spin polarization and to detect the interplay of the magnetic and electronic subsystems, one needs to measure the anomalous Hall effect (AHE), which is proportional to the magnetization and is due to spin-orbit interaction and spin polarization of carriers in DMSs.[2,3] Such measurements play a key role in III-Mn-V DMSs for the identification of the FM state.[2,3] However, in $Si_{1-x}Mn_x$ systems the observation of an AHE displaying a hysteresis loop at sufficiently high temperature (230 K) has been reported up to now only in our paper.[23] Recently, the AHE was also observed in hydrogenated amorphous Si:H with Mn content up to $x \approx 0.35$ at $T \leqslant 150$ K, while the hysteresis loop of the AHE was absent.[24]

In this paper we present the results of magnetic, AHE, and resistivity measurements in $Si_{1-x}Mn_x$ films with a high Mn content ($x \approx 0.35$), which demonstrate the global FM order and indicate that the carrier spin polarization persists at temperatures up to room temperature. A theoretical model is developed to explain the experimental results. This model takes into account the existence of FM angstrom-sized Mn-Si complexes with localized magnetic moments, embedded in the Mn_nSi_m host, which is a weak itinerant ferromagnet.

The paper is organized as follows. The sample characteristics and experimental methods are described in Sec. II. In Sec. III we present the data for the temperature dependence of the resistivity and the Hall effect, mainly the AHE, measurements. The results of the magnetic measurements are presented in Sec. IV; they are in good agreement with the AHE data, which demonstrate the existence of long-range FM order in the systems under study up to room temperature. We show a correlation of the AHE and magnetic properties of the studied films with their conductivity and substrate type. In Sec. V we discuss the experimental results and develop a theoretical model. In Sec. VI we compare the experimental data with theoretical predictions which may explain FM ordering at room temperature in $Si_{1-x}Mn_x$ films, within the framework of our model of the sample structure. A brief summary and conclusion are found in Sec. VII.

II. SAMPLES AND METHODS

$Si_{1-x}Mn_x$ films, mainly of thickness $d = 40–80$ nm, with about 35 at.% of Mn content, were obtained by pulsed laser deposition (PLD) on Al_2O_3 and GaAs substrates under vacuum conditions ($\approx 10^{-6}$ Torr) by the technology described in Ref. 25 for producing $Si_{1-x}Mn_x$ films, although with much smaller Mn content, less than 15%. We used the second harmonic ($\lambda = 532$ nm) of a pulsed Nd:YAG (yttrium aluminum garnet) laser (model LQ 529A). The two laser beams present in the PLD setup are used for the simultaneous ablation of two separated targets of 99.9% pure Mn and float zone Si with dopant concentration $\leqslant 10^{13}$ cm^{-3}. The Mn and Si flows were controlled with the help of a Langmuir probe[26] to obtain the required Mn content; its accuracy was about 10%, estimated by means of electron-probe microanalysis. The deposition rate varied in the range 2.5–5 nm/min. The substrate temperature T_g was mainly stabilized at 300 °C, although some samples were grown at different T_g and with different values of d, to detect how these parameters affect the sample properties. Special attention was paid to the effect of the substrate on transport and magnetic properties of $Si_{1-x}Mn_x$ films. To that purpose, two types of substrate with different lattice parameters were used, Al_2O_3 ($a = 4.76$ Å, $b = 5.12$ Å) and GaAs ($a = 5.66$ Å), with crystallographic orientations (0211) and (100), respectively. For x-ray measurements we used thick samples (sample 7, for example) because the sensitivity was not enough for the thinner ones. These measurements demonstrated that the films under study are manganese silicide polycrystals, with composition close to Mn_4Si_7.[27] Some characteristics of the studied samples are listed in Table I.

TABLE I. $Si_{1-x}Mn_x$ sample parameters.

Sample number	Growth temperature T_g (°C)	Substrate	Film thickness d (nm)	H_c at 80 K (Oe)	AHE at 300 K exceeding (or not) experimental error[a]	AHE sign
1	300	Al_2O_3	40	2900	<	−
2	300	Al_2O_3	57	2000	>	−
3	350	Al_2O_3	55	4200	∼	−
4	300	GaAs	80	0	>	+
5	300	GaAs	50	0	>	+
6	200	GaAs	75	330	<	+
7	300	GaAs	300	650	<	−

[a]Experimental error on Hall resistance is about 10^{-3} Ω at 300 K.

The sample resistivity at room temperature was in the range $(1.3–2.3)\times10^{-4}$ Ω cm, typical for semimetals or heavily doped semiconductors.[28] From the normal Hall effect resistance we found that carriers are of the hole type and their concentration p, estimated from the value of the Hall resistance, is about $p \approx 2\times10^{22}$ cm^{-3}. Usually, the carrier concentration in DMSs is noticeably smaller than the Mn content N_{Mn}, while in our case p is close to the manganese concentration $N_{Mn} \approx 2\times 10^{22}$ cm^{-3} (corresponding to $x \approx 0.35$).

As mentioned above, to detect FM long-range ordering it is really essential to compare magnetic and AHE results. Both magnetic and AHE measurements were performed in the range 4.2–300 K in magnetic field up to 2.5 T. Hall bar samples of size 2×7 mm^2 were prepared for transport measurements; a superconducting interference device, the longitudinal magneto-optical Kerr effect hysteresis, and a vibrating sample magnetometer were used for magnetometry. Magnetic measurements were mainly performed with the magnetic field aligned in the sample plane.

III. RESISTIVITY AND ANOMALOUS HALL EFFECT

The temperature dependence of the resistance $R_{xx}(T)$ for films prepared on Al_2O_3 (samples 2 and 3) and GaAs (samples 4 and 6) substrates is presented in Fig. 1. The $R_{xx}(T)$ dependencies correspond to the metallic type of conductivity

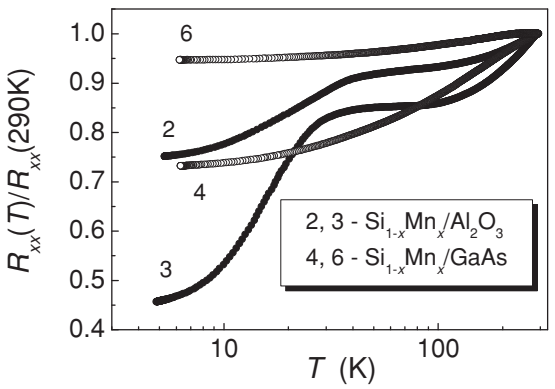

FIG. 1. The temperature dependence of resistivity for $Si_{1-x}Mn_x$ ($x \approx 0.35$) films deposited on Al_2O_3 (samples 2 and 3) and GaAs (samples 4 and 6) substrates. The numbers on the curves are the sample numbers. Growth temperature: 2,4, 300 °C; 3, 350 °C; 6, 200 °C.

and the resistance variation vs temperature is less then 20% when T is decreased from 300 down to 80 K. For samples deposited on the Al_2O_3 substrate at $T_g = 300$ °C the ratio $R_{xx}(290\text{ K})/R_{xx}(80\text{ K})$ is less than 1.1 (samples 1 and 2). On the other hand, the same ratio for samples deposited on the GaAs substrate at the same T_g and of the same thickness is ≈1.2 (samples 4 and 5). This difference in the temperature dependence of the resistance for the two types of samples correlates with the sign of the AHE, which is negative for samples deposited on the Al_2O_3 substrate and positive for samples deposited on the GaAs substrate. With increasing film thickness the crystal structure affects the sample properties more weakly, and for sample 7 (not shown in Fig. 1), deposited on GaAs substrate with thickness 300 nm, $R_{xx}(290\text{ K})/R_{xx}(80\text{ K}) = 1.12$ is closer to the value obtained for samples with Al_2O_3 substrate, and the sign of the AHE is negative. When the temperature of measurements is lowered further, special attention should be paid to the abrupt fall of the resistance at temperatures less than 40 K which is much more pronounced for samples deposited on Al_2O_3 substrates (see Fig. 1). Note that in our case the value $R_{xx}(T)$ changes by less than a factor of 2 in the range 4–50 K, differing drastically from behavior observed in a Mn_4Si_7 single crystal, where the abrupt fall at $T < 50$ K is absent and $R_{xx}(T)$ changes by a factor of 360 in the range 4–300 K.[8] Below, we do not discuss the possible origin of this fall, since the low-temperature region $T < 50$ K is out of the scope of our work. Furthermore, as will be pointed out later, the difference of the $R_{xx}(T)$ dependencies for samples prepared on various substrates correlates with the variation of the AHE and magnetic properties. Nevertheless, the main result obtained, which is the observation of the predominant AHE contribution to the Hall effect at room temperature, is valid for both kinds of sample.

Our main task is to achieve a FM state and the spin polarization of charge carriers in Si-based structures at high enough temperatures, so particular attention should be paid to the interplay of ferromagnetism and electron transport and, in particular, to the AHE. In magnetic materials the Hall resistance R_H is the sum of the normal and anomalous components:

$$R_H d = \rho_{xy} = R_0 B + R_s M;$$

here d is the sample thickness, and R_0 and R_s are constants that characterize the strength of the normal and anomalous Hall resistivities, respectively. The normal Hall effect is related to

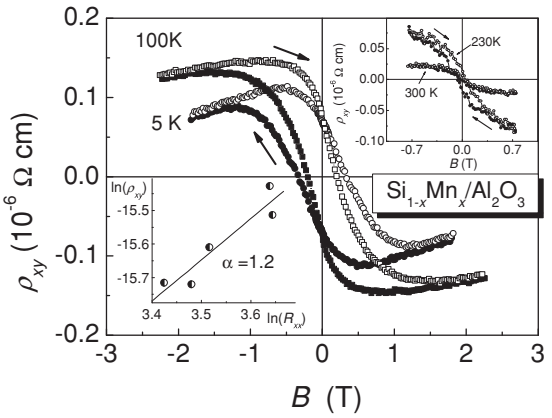

FIG. 2. The Hall effect resistivity hysteresis curves for sample 2 ($Si_{1-x}Mn_x$ /Al_2O_3) at various temperatures. Thick arrows show the magnetic field sweep direction. The upper inset presents the Hall effect resistivity curve at 230 and 300 K. These curves are partly based on results obtained in Ref. 23. The bottom inset shows the dependence $\ln\rho_{xy}$ vs $\ln R_{xx}$, obtained from measurements of the anomalous part of the Hall resistivity ρ_{xy} and resistance R_{xx} at $T < 100$ K.

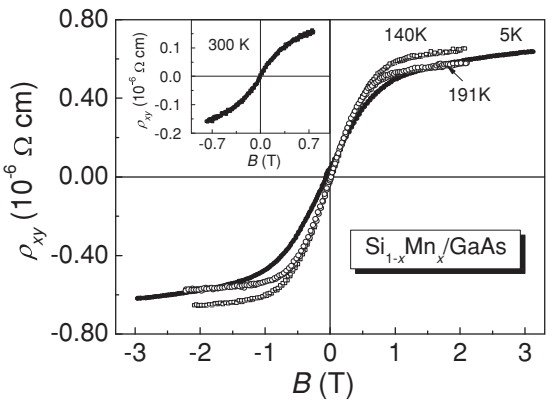

FIG. 3. The Hall effect resistivity versus magnetic field for sample 4 ($Si_{1-x}Mn_x$/GaAs) at various temperatures. Inset: the room temperature data.

the Lorentz force and is proportional to the magnetic induction B, whereas the AHE is proportional to the magnetization M and is determined by the spin-orbit interaction and spin polarization of the carriers. $R_s \propto (R_{xx})^\alpha$, where $\alpha = 1$ for the "skew-scattering" mechanism of AHE and $\alpha = 2$ for "intrinsic" and "side-jump" mechanisms.[2]

The curves $\rho_{xy}(B)$ for samples 2 and 4 deposited on Al_2O_3 and GaAs substrates and having the same ratio $R_{xx}(290\ \text{K})/R_{xx}(5\ \text{K}) = 1.3$–$1.4$ are shown in Figs. 2 and 3, respectively, at different temperatures up to room temperature [the upper inset in Fig. 2 shows the magnetic field dependence of the Hall resistivity, $\rho_{xy}(B)$, for sample 2 at high temperatures 230 and 300 K in fields $\leqslant 1$ T]. For both samples the Hall resistance depends nonlinearly on the magnetic field, proving the existence of the anomalous components of the Hall effect, while at high fields the crossover to the linear dependence $\rho_{xy} \propto B$ (normal Hall effect) is observed. Based on the data presented in Figs. 2 and 3, one could argue that in all samples the Hall effect is anomalous at temperatures much higher than the temperature of magnetic ordering in Mn_4Si_7 (43 K). Furthermore, the anomalous component of the Hall effect is predominant up to room temperature in both types of structure, being, however, noticeably stronger for samples deposited on GaAs substrates than for samples with Al_2O_3 substrates.

It should be stressed that we have observed an AHE hysteresis loop (see Table I and Fig. 2). For sample 2 the dependence $\rho_{xy}(B)$ shows a rather strong coercive field $H_c \approx 2$ kOe at $T \approx 100$ K ($H_c = B_c/\mu_0$) and the hysteresis loop persists up to rather high temperature ≈230 K (see upper inset in Fig. 2). In previous studies of $Si_{1-x}Mn_x$ structures, the anomalous component of the Hall effect was not observed,[16,18,19] or the AHE did not show a hysteresis loop.[24] To our knowledge, the hysteresis loop of the AHE at such high temperatures is observed here for the first time in Si-based DMSs.

The behavior of the AHE is different for various substrates, its sign being mainly negative for $Si_{1-x}Mn_x/Al_2O_3$ and positive for $Si_{1-x}Mn_x$/GaAs. Noticeably also the coercive field for samples prepared on Al_2O_3 substrates is much higher then that in $Si_{1-x}Mn_x$/GaAs samples. For example, in sample 4 the hysteresis is absent (see Fig. 3), while in sample 2 the value of B_c is quite large (see Fig. 2). The absence of coercive field for the AHE in $Si_{1-x}Mn_x$/GaAs is due to the anisotropy of the magnetic moment, which could be aligned within the sample plane, in contrast to the case of samples prepared on Al_2O_3 substrates. Such a statement is in agreement with the results of magnetization measurements (see Sec. IV). The difference of the magnetic anisotropy in samples prepared on different substrates could be due to the variation of crystallite orientations determined by the substrate structure or to the possible strain arising in films. For example, the magnetic moment for $Ga_{1-x}Mn_xAs$/GaAs lies in the sample plane, but for the same samples prepared on $In_{0.16}Ga_{0.84}As$ it is perpendicular to this plane.[29] The results for sample 7 do not contradict the above mentioned tendencies because this sample is very thick (300 nm, about five times thicker than other samples), and the effect of the substrate on the sample is weaker.

To shed light on the mechanism of the AHE one could analyze the parametric dependence $R_s(R_{xx})$. As mentioned earlier, the theory predicts $R_s \propto (R_{xx})^\alpha$ with $\alpha = 1$ for skew scattering and $\alpha = 2$ for the side-jump or intrinsic mechanisms.[2] However, recently an empirical scaling relation of the AHE ($\sigma_{xy}^a \propto \sigma_{xx}^{1.6}$) was found for ferromagnetic materials with not very high conductivity[30] (in our case σ_{xx} is $\approx 10^4\ \Omega^{-1}$ cm^{-1}). Usually, the parameter α could be estimated from the $\rho_{xy}(R_{xx})$ dependence using the temperature as a parameter under the condition $M(T) = \text{const}$. For samples 1 and 2, grown at $T_g = 300\ ^\circ\text{C}$, the estimated values of α fall in the range indicated above (see the bottom inset in Fig. 2). However, we do not take into account the temperature dependence of magnetization. In addition, changes in longitudinal resistance R_{xx} in our case are rather small and introduce some noise in the dependence $\rho_{xy}(R_{xx})$ (Fig. 2). So there is insufficient data to discriminate definitely between various AHE mechanisms.

Finally, the difference in the sign of the AHE for $Si_{1-x}Mn_x/Al_2O_3$ and $Si_{1-x}Mn_x$/GaAs is not related to the sign of the charge carriers, because they are holes in both cases, and rather is due to the AHE mechanism, because the sign of

R_s can be positive or negative depending on the material band structure, on the subtle interplay between the orientations of orbital and spin moments, and on the character (repulsive or attractive) of the scattering potentials.[3] For instance, the sign of the AHE is positive for Fe, whereas it is negative for Ni.[28]

IV. MAGNETIZATION

Let us now compare the AHE results with those obtained from magnetization measurements. The magnetic field dependencies of the magnetization $M(H)$ for the $Si_{1-x}Mn_x/Al_2O_3$ structure (sample 2; the area of the sample $S \approx 2\times4$ mm^2) and for the $Si_{1-x}Mn_x$/GaAs structure (sample 4; $S \approx 2\times5$ mm^2), measured at various temperatures with field parallel to the sample plane are presented in Figs. 4(a) and 4(b), respectively. It is seen from the data presented in Fig. 4(a) that the magnetization signal is observed up to 300 K. The saturation magnetization at 80 K is ≈12 emu/cm^3. The $M(B)$ dependence displays a hysteresis. The coercivity H_c at 80 K is ≈1.2 kOe. At saturation the magnetic moment per Mn atom for these samples is ≈0.07 μ_B/Mn and ≈0.03 μ_B/Mn for $T = 200$ and 300 K, respectively.

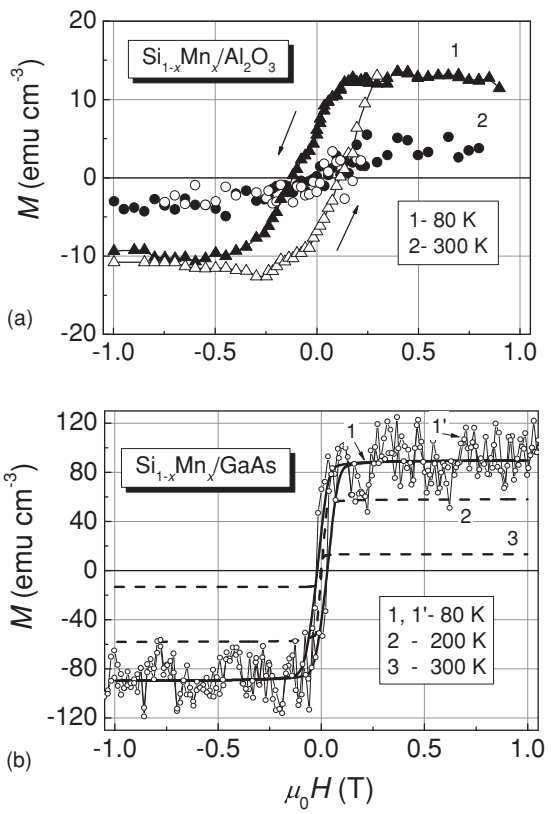

FIG. 4. The magnetization hysteresis curves for sample 2 ($Si_{1-x}Mn_x/Al_2O_3$) (a) and sample 4 ($Si_{1-x}Mn_x$/GaAs) (b) at various temperatures. Arrows show the magnetic field sweep direction. The hysteresis loops for the samples on the GaAs substrate are considerably narrower than for $Si_{1-x}Mn_x/Al_2O_3$ structures; therefore the measured $M(H)$ curves for sample 4 have been fitted with a Langevin function for obtaining the coercivity H_c. Curves 1–3 correspond to the fitted dependencies $M(H)$ at 80, 200, and 300 K. The measured dependence $M(H)$ for 80 K is shown (curve 1′).

The magnetic moment of sample 4 ($Si_{1-x}Mn_x$/GaAs structure) is well observed at room temperature [see Fig. 4(b)]. However, the hysteresis loops for the samples on GaAs substrates are considerably narrower than those found in the $Si_{1-x}Mn_x/Al_2O_3$ structures. Therefore, the measured $M(H)$ curves have been fitted with a Langevin function to obtain the coercivity H_c [the measured dependence $M(H)$ at $T = 80$ K is shown in Fig. 4(b) with curve 1′; in turn the curves 1–3 correspond to the fitted dependencies $M(H)$ at 80, 200, and 300 K]. Specifically, the value of coercivity H_c obtained with this fitting procedure for sample 4 at 80 K is about 240 Oe. The saturated value of the magnetic moment per Mn atom for this particular sample is ≈ 0.3 μ_B/Mn at $T = 200$ K (≈ 0.08 μ_B/Mn for $T = 300$ K) and exceeds the value found in samples 1 and 2. So the magnetic moment per Mn atom depends on the substrate and it is several times larger for samples prepared on GaAs substrates than for samples on Al_2O_3 substrates. The values obtained are more than one order of magnitude larger than the magnetic moment in Mn_4Si_7 (≈0.012 μ_B/Mn),[8] and four times larger than that in $Si_{1-x}Mn_x$ films with lower Mn content, 3.6–5.5 at.%,[19] in which the moment is equal to (0.03–0.05)μ_B/Mn at 200 K. It is seen that the coercivity of the samples deposited on GaAs is much smaller than for samples with Al_2O_3 substrates, while the opposite holds for the value of M_s [see Figs. 4(a) and 4(b)]. The same fact is valid for the AHE results: samples with GaAs substrates to all practical extent do not show hysteresis, but the AHE at saturation is about a factor of 5 larger than in $Si_{1-x}Mn_x/Al_2O_3$ structures.

For both samples 2 and 4, the coercivity and saturation moment diminish when the temperature increases, as is expected.

Some magnetization measurements were performed for sample 2 ($Si_{1-x}Mn_x/Al_2O_3$) with field perpendicular to the sample plane. The results are comparable with those obtained in parallel field; the saturated M_s magnetic moments are of the same value in both cases. Also the coercivity extracted from the AHE (perpendicular field) and magnetization (parallel field) measurements are in agreement with each other; for example, at 80 K, $H_c \approx 1.2$ kOe in both cases. Using the equation $H_c \approx 2K/M_s$, where K is the anisotropy constant, and the experimental data $H_c \approx 10^3$ Oe and $M_s \approx 10$ emu/cm^3 (see Fig. 4), one can obtain that the anisotropy is weak, $K \approx 5\times10^3$ erg/cm^3, while the shape anisotropy is even much smaller, being determined by $M_s^2 = 10^2$ erg/cm^3. Based on the data presented above, it is natural to suggest that the sample structure consists of crystallites with uniaxial anisotropy which are randomly oriented, resulting in a nearly isotropic behavior of the sample. Growth parameters affect the crystallite anisotropy; for example, for the sample 3, $M_r/M_s \approx 1$, while for structures with GaAs substrate (samples 4–6) the coercivity is practically absent for the AHE, whereas a small coercivity exists for the magnetic moment [compare Figs. 4(a) and 4(b)]. The latter could be due to the alignment of the magnetic moment in the sample plane for this particular structure. With increasing sample thickness the influence of the substrate becomes weaker. Accordingly, sample 7, grown on GaAs substrate with $d \approx 300$ nm, displays a quite large H_c, determined from the magneto-optical Kerr effect measurements (see below), and negative AHE sign, in contrast to other $Si_{1-x}Mn_x$/GaAs samples.

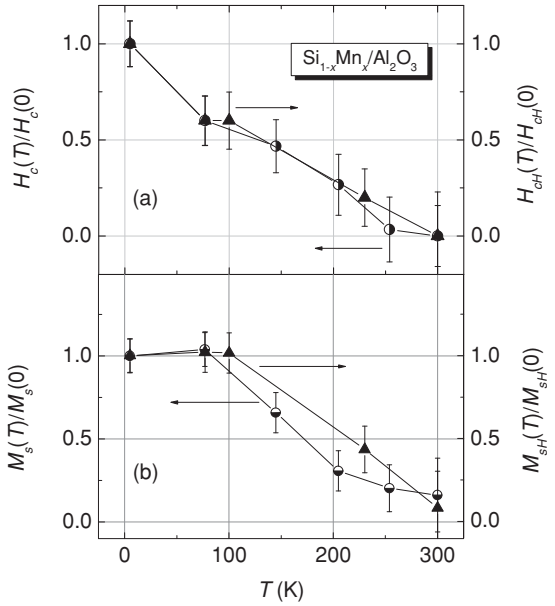

FIG. 5. The normalized coercivity $H_c(T)/H_c(0)$ (a) and saturation magnetization $M_s(T)/M_s(0)$ (b) obtained from both transport (triangles) and magnetic measurements (circles) for sample 2 ($Si_{1-x}Mn_x/Al_2O_3$). $H_c(0)$ and $M_s(0)$ are the low (helium) temperature values. $M_s(T)$, $H_c(T)$ and $M_{sH}(T)$, $H_{cH}(T)$ are the magnetization and coercivity values calculated from magnetic measurements and Hall effect measurements, respectively.

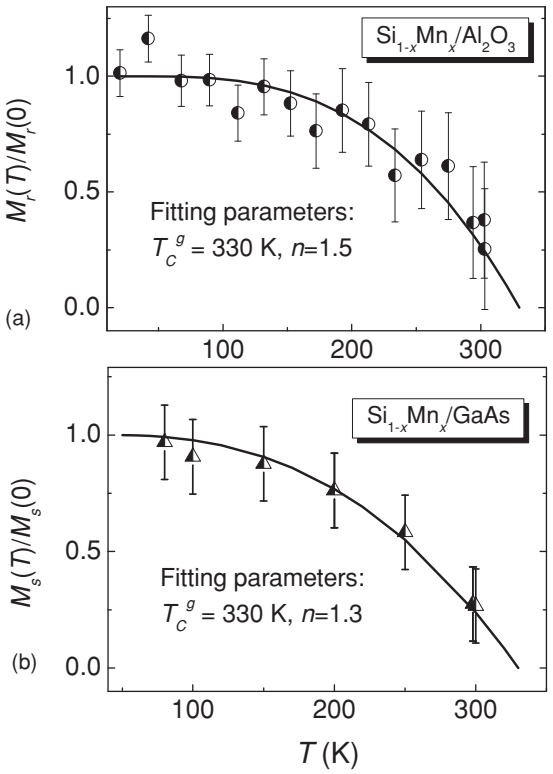

FIG. 6. Temperature dependences of normalized remanent magnetization $M_r(T)/M_r(0)$ for sample 2 ($Si_{1-x}Mn_x/Al_2O_3$) (a) and normalized saturation magnetization $M_s(T)/M_s(0)$ for sample 4 ($Si_{1-x}Mn_x$/GaAs) (b). For sample 4 the $M_s(T)/M_s(0)$ dependence is presented instead of $M_r(T)/M_r(0)$ because the hysteresis loop for $Si_{1-x}Mn_x$/GaAs samples is very narrow and the remanent magnetization could not be evaluated with sufficient accuracy. The $M_s(T)$ value was measured at $B = 0.5$ T. Magnetizations $M_r(0)$ and $M_s(0)$ correspond to $T = 4.2$ K. The solid lines are the fitting of temperature dependencies for $M_r(T)/M_r(0)$ and $M_s(T)/M_s(0)$ by the theoretically obtained function $F(y) = 1-y^n$ with $y = T(T - T_C^h)/T_C^g(T_C^g - T_C^h)$ and $T_C^h = 50$ K related to the model discussed in Sec. V (see also Sec. VI). Fitting parameters are $T_C^g = 330$ K for both curves, and n is 1.5 and 1.3 for sample 2 and sample 4, respectively.

The above mentioned results of the magnetization measurements are in agreement with the $\rho_{xy}(B)$ dependence, as may be seen from comparison of the results presented in Fig. 2 with Fig. 4(a) and in Fig. 3 with Fig. 4(b). The magnetic field dependences of $\rho_{xy}(B)$ and $M(B)$ are close to each other and show similar hysteresis. In particular, for sample 2 the coercivity measured by magnetization measurements is approximately the same as that obtained from the AHE. Furthermore, the temperature dependences of the coercivity obtained from transport and magnetic measurements also agree very closely, as may be seen from Fig. 5(a), where the temperature dependences of the normalized coercivity $H_c(T)/H_c(0)$ obtained from both transport and magnetic measurements are presented [$H_c(0)$ is the low-temperature value].

The temperature dependence of the saturation magnetization $M_s(T)/M_s(0)$ measured at $B = 1$ T is shown in Fig. 5(b). Here, $M_s(0)$ is the value of M_s measured at low temperatures. In this figure, the analogous data extracted from the AHE measurements are also shown. To obtain the ratio between the saturation magnetization at temperature T and at zero temperature from the AHE results, one should take into account the AHE resistance $R_H^A = R_s M$, where R_s also depends on T, following the temperature dependence of $R_{x,x}$, i.e., $R_s \propto (R_{xx})^\alpha$, where in our case mainly $\alpha \cong 1$. Hence, we have

$$R_{Hs}^A(T)/R_{Hs}^A(0) = [R_s(T)/R_s(0)][M_H(T)/M_H(0)] = [R_{xx}(T)/R_{xx}(0)]^\alpha [M_H(T)/M_H(0)],$$

where the index H for M means that the magnetic moment is extracted from the AHE measurements. The temperature dependence of $M_{sH}(T)/M_{sH}(0)$, where M_{sH} is the saturated value of M_H, is presented in Fig. 5(b) and compared with $M_s(T)/M_s(0)$.

The Curie temperature for sample 2 could be estimated as about 300 K from the temperature dependence of the residual magnetization M_r, which is shown in Fig. 6(a). As seen from Fig. 6(b) for sample 4, the Curie temperature is also slightly higher than 300 K. The experimental data presented in these figures are fitted with the theoretical expression obtained in Sec. V (see also Sec. VI). For the $Si_{1-x}Mn_x$/GaAs sample 7, of larger thickness, magneto-optical Kerr effect measurements were performed, showing hysteresis with H_c about 0.7 kOe at $T \leqslant 80$ K (see Fig. 7).

The anomalous contribution to the Hall resistivity $\rho_{xy}^a(B)$ can be obtained from $\rho_{xy}(B)$ by subtraction of the normal component of the Hall effect, which in turn can be found at magnetic fields above saturation. From the magnetization values we determined the coefficient of the AHE,

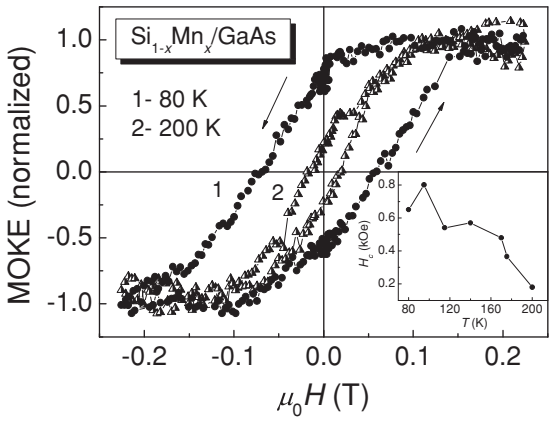

FIG. 7. Hysteresis curves for normalized magneto-optical Kerr effect for sample 7 ($Si_{1-x}Mn_x$/GaAs) taken at temperatures 80 K (curve 1, circles) and 200 K (curve 2, triangles). Arrows show the magnetic field sweep direction. Inset: Temperature dependence of the coercivity.

$R_s = \rho^a_{xy}/M$, which is about 10^{-8} Ω cm/G for sample 2 (Al_2O_3 substrate) at $T = 80$ K. A similar value, $R_s \sim 0.7\times10^{-8}$ Ω cm/G, was obtained for sample 4 (GaAs substrate) at room temperature.

The AHE angle tangent $\beta = \rho^a_{xy}/\rho_{xx}$ at 200 K is about 5×10^{-3}, the hint of the spin polarization of carriers. To draw any conclusion about the reason for the Hall effect anomaly in our sample we employed the relation $\rho_{xy}/\rho_{xx} = \mu B + \beta M/M_S$, where μ is the carrier mobility.[3] The Hall effect anomaly could also be caused by magnetic precipitates, whose stray fields ($B_{st} \leqslant 4\pi M_S$) may produce an apparent magnetization-dependent contribution to the Hall resistance. However, in our samples the carrier mobility is less then 5 cm^2/V s and so to observe at zero external field a value $\beta \approx \mu B_{st} \approx 5\times10^{-3}$, a stray magnetic field exceeding 10 T would be needed, which is unrealistic for magnetic precipitates ($B_{st} < 0.7$ T at manganese concentration $N_{Mn} < 2\times10^{22}$ cm^{-3} and the effective magnetic moment $<3\mu_B$/Mn). Thus, following Ref. 3, we may conclude that in our case the spin polarization of carriers under their spin-orbit interactions totally controls R_S.[3]

V. DISCUSSION OF THE EXPERIMENTAL RESULTS AND THEORETICAL MODEL

The experimental results obtained in Secs. II–IV clearly demonstrate that FM order with an effective magnetic moment per Mn atom ($\approx0.2\mu_B$/Mn) was observed at fairly high temperatures in $Si_{1-x}Mn_x$ alloys with large manganese content ($x \approx 0.35$). The origin of this FM order is, however, not evident and has to be discussed.

As anticipated in Sec. I, the AHE (see Figs. 2 and 3) and magnetization (Figs. 4 and 5) properties, as well as the high values of T_C, could not be attributed to the bulk manganese silicides Mn_nSi_m with ratio m/n ranging between 1.70 and 1.75 (e.g., Mn_4Si_7, $Mn_{11}Si_{19}$, $Mn_{15}Si_{26}$, $Mn_{26}Si_{45}$, $Mn_{27}Si_{47}$). Indeed, the Curie temperature T_C in these materials does not exceed 50 K and the effective magnetic moment per Mn atom is extremely small (for example ≈0.012 μ_B/Mn in Mn_4Si_7,[8] i.e., significantly smaller than in the alloys under study). In these silicides, the 3*d* states of Mn are strongly hybridized with the 4(*s*,*p*) states of Si, so the spin density on the Mn atom is almost completely delocalized. Therefore, these materials are classified as exchange-enhanced paramagnets or weak itinerant ferromagnets. First-principle calculations showed that the different silicides Mn_nSi_m are semiconducting, metallic, or half metallic.[9] For instance, spin-polarized calculations for $Mn_{11}Si_{19}$, $Mn_{15}Si_{26}$, and $Mn_{27}Si_{47}$ showed that these phases are half metallic, with full spin polarization of holes at the Fermi level, whereas the ideally stoichiometric and unstressed Mn_4Si_7 turns out to be a semiconductor, with indirect band gap, although small nonstoichiometry or stress can lead to the closure of the gap, transforming the material into a metal. Due to the helicoidal long-period character of FM order in Mn_nSi_m (see Refs. 14 and 21), the hysteresis loop might be absent or very small even at $T < T_c$. Note also that the temperature dependence of the resistivity $R_{xx}(T)$ in Mn_4Si_7 differs drastically from the one we have observed. Indeed, for Mn_4Si_7 R_{xx} diminishes by more than 50 times in the temperature range between 300 and 80 K and saturates at $T \leqslant 20$ K. In this case, the ratio $R_{xx}(290\text{ K})/R_{xx}(5\text{ K})$ reaches a value as high as 360, while in our sample this ratio is at most ≈2. Furthermore, in our samples, R_{xx} weakly depends on temperature in the interval $80 < T < 300$ K, and $R_{xx}(T)$ abruptly decreases at $T \leqslant 40$ K for samples prepared on Al_2O_3 substrates (see Fig. 1).

Recently, we proposed a possible theoretical mechanism for high-temperature ferromagnetic order in Si:Mn dilute alloys,[31] which are suggested to undergo phase separation. In the phase-separated state, Mn atoms can be gathered within Mn-rich precipitate particles which are embedded in the Mn-poor silicon matrix. We considered the precipitate to be the Mn_nSi_m silicide host containing a certain amount of magnetic defects associated with unbound Mn 3*d* orbitals. The Mn_nSi_m silicide was supposed to be a weak itinerant ferromagnet, where sizable spin fluctuations (paramagnons) exist far above its intrinsic Curie temperature. In the framework of the "local phase transition" approach,[32] relying on Moriya's spin fluctuations theory[33] and on the Murata-Doniach approximation of noninteracting spin modes,[34] we suggested that the Stoner enhancement of the exchange interaction between local magnetic moments of defects takes place, mediated by spin fluctuations in the host. The general possibility of such an enhancement in GaMnAs DMSs was first mentioned in Ref. 35. As a result, a significant increase of the "global" Curie temperature of the system occurs.

In this work we use the theoretical model of Ref. 31, adapted to deal with macroscopically homogeneous concentrated Si:Mn alloys without phase segregation, to qualitatively explain the experimental results obtained above. It is reasonable to assume that these alloys have a microscopic structural disorder, so the lack of local order around the Mn site can provide partial localization of Mn 3*d* states. The $Si_{1-x}Mn_x$ ($x \approx 0.35$) material is believed to include angstrom-sized magnetic defects (single Mn ions or molecular complexes containing Mn), denoted henceforth by the symbol Mn_D. We suppose, for concreteness, that these defects have magnetic configurations corresponding to substitutional or interstitial positions in the Si lattice,[17] where they have an effective

magnetic moment ≈(2–3)μ_B/Mn atom. We distinguish two different components in the spin density of $Si_{1-x}Mn_x$ alloys: an itinerant (delocalized) component inherent to a Mn_nSi_m weak ferromagnet and a localized component specific to the Mn_D defects. According to the suggestion that our alloy consists of a Mn_nSi_m matrix and of Mn_D defects embedded in it, we may assume that the chemical formula of our material is $(Mn_nSi_m)_{1-\lambda}(Mn_D)_\lambda$. For concreteness, let us describe the Mn_nSi_m host as the Mn_4Si_7 silicide. Thus, the $Si_{1-x}Mn_x$ alloy with nominal Mn content $x \approx 0.35$ could be formally regarded as a material with the formula $MnSi_{1.86}$, while Mn_4Si_7 could be formally represented as the $MnSi_{1.75}$ silicide. The identification $MnSi_{1.86} = (MnSi_{1.75})_{1-\lambda}(Mn_D)_\lambda$ can easily explain the difference between the effective magnetic moment per Mn atom observed in our films (≈0.2 μ_B/Mn) and that observed in Mn_4Si_7 (≈0.012 μ_B/Mn). The effective magnetic moment per Mn atom in the Mn_D defect is about 2.54 μ_B/Mn for the Mn_T (interstitial) center, 2.0 μ_B/Mn for the $Mn_{Si}-Mn_T$ (substitutional-interstitial) dimer, and 2.7 μ_B/Mn for the Mn_T-Mn_T (interstitial-interstitial) dimer,[17] being somewhat less than the "nominal" value ≈(4–5)μ_B/Mn for Mn atoms in a GaAs host.[2] Having this value and the measured effective magnetic moment per Mn atom, the amount of Mn atoms that do not belong to the host matrix and instead form magnetic defects can be evaluated as ≈(8–10)% of the total Mn content in the $Si_{1-x}Mn_x$ film. For the $Si_{1-x}Mn_x$ alloy with x ≈0.35 and total Mn concentration $N_{Mn} \approx 2 \times 10^{22}$ cm^{-3}, the concentration of magnetic defects may be estimated as $N^D_{Mn} \approx (0.8-1.8) \times 10^{21}$ cm^{-3}. This value corresponds to a mean distance between defects $a_0 \approx$ 10–12 Å. One could also estimate the number of Si atoms per molecular complex, $Z^D_{Si} \approx$4–5. Obviously, our estimates are rough and the different properties of samples prepared on various substrates may be accounted for by the crystal structure of the matrix imposed by the substrate. In turn, variations in the structure of the matrix could affect the concentration, size, and shape of the magnetic defects.

Obviously, serious problems arise in trying to explain high-temperature ferromagnetism in our system. Indeed, such a small concentration of defects carrying magnetic moments is inadequate to promote FM order at high temperatures within the Ruderman-Kittel-Kasuya-Yosida (RKKY)/Zener model of exchange coupling. The main reason is that the above estimated mean distance between magnetic defects is on the order of the period of RKKY oscillations: $2k_Fa_0 \geqslant 10$, where $k_F^{-1} \approx 1-1.5$ Å is the inverse Fermi wave vector. So the spin-glass regime would be more realistic in this situation, at odds with the observed FM behavior.

Following the model developed in Ref. 31, one can show that the effective Hamiltonian H^{SF}_{ex} of coupling between local magnetic moments of Mn_D defects in the Mn_nSi_m host mediated by spin fluctuations (SF) has the form

$$H^{SF}_{ex} = \frac{1}{2}\sum_{i\neq j} J^{SF}_{ij}\mathbf{S}_i\mathbf{S}_j, \quad J^{SF}_{ij} \approx -J_0\frac{\exp(-a_{ij}/\zeta)}{k_Fa_{ij}}, \qquad (1)$$

where $\mathbf{R}_i$ and $\mathbf{S}_i$ are the random position and magnetic moment for the ith defect, respectively, $a_{ij} = |\mathbf{R}_i - \mathbf{R}_j|$ is the distance between defects, $\zeta(T)$ is the correlation length of paramagnons in the host, which depends on the temperature, and $J_0 > 0$ is the amplitude of exchange coupling defined by the microscopic parameters of the system. In particular, for the standard model of an indirect p-d exchange between the local d-electron spin and itinerant p-electron spin in the metal, one can estimate $J_0 \propto J^2_{pd}/W$, where J_{pd} is the integral of p-d exchange, W is the energy on the order of the p-electron bandwidth, $W \propto v_Fk_F$, where v_F is the Fermi velocity. The coupling integral J^{SF}_{ij} is always ferromagnetic and has an exponential falloff at large distances, $a_0 > \zeta > k_F^{-1}$. Thus, at extremely low concentration of defects their coupling through spin fluctuations seems to be negligible. However, at intermediate distances, $k_F^{-1} < a_0 \sim \zeta$, the contribution (1) may exceed or be comparable in order of magnitude to the integral J^{RKKY}_{ij} in the RKKY mechanism of exchange coupling, $|J^{RKKY}_{ij}| \propto (k_Fa_{ij})^{-3}$. This means that, even in systems with a relatively low concentration of defects, and obviously with a higher concentration ($k_F^{-1} < a_0 < \zeta$), the contribution (1) has to be taken into account.

In order to evaluate the temperature of the ferromagnetic ordering of local magnetic moments, T^g_C (we call it the *global* Curie temperature), one can use the Weiss molecular field approximation:

$$T^g_C = \frac{S^2}{3k_B}J^{SF}_0(T^g_c),$$
$$J^{SF}_0(T^g_c) = -\sum_j J^{SF}_{ij}(T^g_C) \approx N^D_{Mn}4\pi J_0k_F^2\zeta^2. \qquad (2)$$

At $T^g_C \gg T^h_C$, where T^h_C is the *intrinsic* Curie temperature of the host, following Ref. 31, one can evaluate $\zeta(T^g_C) \approx v_F/\sqrt{Wk_BT^g_C}$, where $W \approx 4-6$ eV, which is a typical value for 3d bands in manganese silicides,[9] and k_B is the Boltzmann constant. At $a_0 \approx 10-12$ Å and $k_F^{-1} \approx 1-1.5$ Å (for typical carrier concentrations $n \approx 10^{22}$ cm^{-3}) the regime $a_0 \approx \zeta \gg k_F^{-1}$ is easily achieved, and for the temperature T^g_C we can write

$$k_BT^g_C \approx \sqrt{WS^2N^D_{Mn}4\pi J_0}/3 \approx \sqrt{Wk_BT^{RKKY}} \gg k_BT^{RKKY}, \qquad (3)$$

where $k_BT^{RKKY} \approx J_0N^D_{Mn}4\pi S^2/3k_B$ and T^{RKKY} is the Curie temperature in the RKKY model at the same concentration of magnetic defects, N^D_{Mn}. Even adopting the cautious estimate $T^{RKKY} \approx 10$ K at very low concentration of defects, we obtain $T^g_C \geqslant 600$ K. Obviously, in real alloys the effect of structural disorder will further reduce this estimate.

VI. COMPARISON OF THEORETICAL PREDICTIONS WITH EXPERIMENTAL RESULTS

First of all, let us point out that the model of exchange (henceforth called the SF model) presented above yields an estimated Curie temperature which is in agreement with experimental values, in contrast to the standard RKKY/Zener model of exchange which predicts the spin-glass regime. The SF model leads to a sizable growth of the Curie temperature in our system, with respect to the case when only the standard RKKY-like mechanism is taken into account.

In the frame of the SF model, the temperature dependence of the magnetization $M(T)$ should differ from that obtained within the RKKY theory. In the RKKY model, the mean-field value

of the exchange integral J^{RKKY} does not depend on temperature, while the SF model yields $J^{SF}(T) \propto (T - T_C^h)^{-1}$. The equations describing the temperature dependence of the mean magnetization, $M(T)$, contain the factors J^{RKKY}/T in the frame of the RKKY model or $J^{SF}(T)/T$ in the frame of the SF model. So, if the RKKY model fits the $M(T)$ dependence by the function $F(T/T_C)$, then the SF model exploits the same function, but with a different argument, $T(T - T_C^h)/T_C^g(T_C^g - T_C^h)$, to fit the $M(T)$ curve; as a result, for $T > T_C^h$ we have $M(T)/M(T_C^h) \approx F[T(T - T_C^h)/T_C^g(T_C^g - T_C^h)]$.

It is known that, in DMSs, the spatial disorder modifies the $M(T)$ dependence[36] (in particular, for the case of standard RKKY theory, see Ref. 37). Under the effect of disorder, the $M(T)$ dependence differs from that described by the Brillouin equation and could be fitted by the function $F(y) = 1 - y^n$, with $y = T/T_C$ [in particular, $n \approx 2$ for GaMnAs (Ref. 38)]. In the SF model, the experimental dependence $M(T)$ can be fitted with the same function $F(y)$, but with $y = T(T - T_C^h)/T_C^g(T_C^g - T_C^h)$ [see Figs. 6(a) and 6(b)]. Taking $n = 1.3$–1.5 and $T_C^h = 50$ K, we obtain the *fitted* Curie temperature $T_C^g(\mathrm{fitted}) \approx 330\,\mathrm{K}$ for both samples 2 and 4, in good agreement with the prediction of the SF theory, $T_C^g \approx 300-500$ K.

It should be mentioned that it is very hard to explain the observed results of the AHE and magnetic measurements based on the bulk $\mathrm{Mn}_n\mathrm{Si}_m$ properties. On the contrary, these results, as well as the data of resistivity measurements, are in qualitative agreement with the model proposed here for the sample structure: magnetic defects (FM molecular clusters) embedded in the $\mathrm{Mn_4Si_7}$ matrix. Indeed, in the whole temperature range $R_{xx}(T)$ differs drastically from its behavior in $\mathrm{Mn}_n\mathrm{Si}_m$; furthermore at the temperature of magnetic ordering for the host Mn silicide, T_C^h, the curve $R_{xx}(T)$ abruptly decreases. Also the sample characteristics depend on the substrate type, which affects the matrix structure, but the main magnetic properties (magnetic moment, existence of the AHE) do not change significantly.

VII. CONCLUSIONS

Room-temperature ferromagnetism has been achieved in Si-based structures with high Mn content. The important point is that the FM behavior was detected not only by magnetization measurements but also by the observation of the anomalous Hall effect. So FM order involves charge carriers which are most probably at least partially spin polarized, and is not due to separated magnetic inclusions not interacting with carriers. The magnetic hysteresis loop as well as the temperature dependence of the saturation magnetization and coercive field measured by magnetic and transport methods are similar, and this fact proves the previous statement. The Curie temperature obtained from the temperature dependence of residual magnetization was found to be about 330 K. It is hard to explain the whole set of experimental results in the frame of the standard RKKY/Zener model of exchange between local moments of manganese, or by the formation of a weak itinerant ferromagnet (manganese silicide) in the $\mathrm{Si}_{1-x}\mathrm{Mn}_x$ ($x \approx 0.35$) alloy under consideration.

To explain the experimental data, we used a more complex model of FM order, based on the conception of a two-phase magnetic material composed of defects with local magnetic moments, which are embedded in the host, assumed to be a weak itinerant ferromagnet. We argued that molecular clusters (probably $\mathrm{Mn_{Si}}-\mathrm{Mn}_T$ or Mn_T-Mn_T dimers), containing a minority of Mn atoms, form these defects in our alloy, while the majority of Mn atoms is involved in the formation of the $\mathrm{Mn}_n\mathrm{Si}_m$ host. In our opinion, the observed FM ordering at high temperatures (>300 K) is due to the Stoner enhancement of the exchange coupling between local moments of defects provided by strong spin fluctuations ("paramagnons") in the host. We described this enhancement at a phenomenological level using a model of a weak itinerant ferromagnet far above its intrinsic Curie temperature. The important role of long-wavelength (on the order of a correlation length) collective excitations (paramagnons) is revealed for the SF model of coupling, leading to its nonoscillatory character, whereas short-wavelength (on the order of the Fermi wavelength) one-electron excitations dominate in the RKKY model of coupling, leading to its oscillatory behavior. We demonstrated that the SF model does not contradict the experimental data, when model parameters of a plausible order of magnitude are used. Obviously, in $\mathrm{Si}_{1-x}\mathrm{Mn}_x$ alloys both components of exchange coupling coexist, but their relative contribution may vary from the one-electron (RKKY) regime to the collective (SF) regime, depending on the Mn content and growing conditions.

ACKNOWLEDGMENTS

We thank C. Back, A. V. Vedyaev, A. B. Granovskii, and E. Z. Meilikhov for fruitful discussions. V.V.T. thanks the Basque Foundation for Science (Ikerbasque) and Donostia International Physics Center (DIPC) for organization and financial help. B.A. thanks S. Ganichev and C. Back for hospitality and the University of Regensburg for financial support. The work is partially supported by RFBR (Grants No. 08-02-01462, No. 09-02-12108, No. 09-07-12151, No. 09-07-13594, No. 10-07-00492, and No. 10-02-00118) and RNP Grant No. 2.1.1/2833. S.C. acknowledges financial support by PRIN under Project No. 2007FW3MJX003.

*aronzon@imp.kiae.ru
†vvrylkov@mail.ru
‡tuvictor@mail.ru
§sergio.caprara@roma1.infn.it

[1] *Semiconductor Spintronics and Quantum Computation*, edited by D. D. Awschalom, D. Loss, and N. Samarth (Springer, Berlin, 2002).

[2] T. Jungwirth, Jairo Sinova, J. Mašek, J. Kučera, and A. H. MacDonald, Rev. Mod. Phys. **78**, 809 (2006); K. Sato, L. Bergqvist, J. Kudrnovský, P. H. Dederichs, O. Eriksson, I. Turek, B. Sanyal, G. Bouzerar, H. Katayama-Yoshida, V. A. Dinh, T. Fukushima, H. Kizaki, and R. Zeller, *ibid.* **82**, 1633 (2010).

[3]T. Dietl, in *Modern Aspects of Spin Physics*, Lecture Notes in Physics, edited by Pötz, Walter, Fabian, Jaroslav, Hohenester, and Ulrich, Vol. 712 (Springer-Verlag, Berlin, Heidelberg, 2007), pp. 1–46.

[4]R. P. Panguluri, K. C. Ku, T. Wojtowicz, X. Liu, J. K. Furdyna, Y. B. Lyanda-Geller, N. Samarth, and B. Nadgorny, Phys. Rev. B **72**, 054510 (2005).

[5]P. Van Dorpe, Z. Liu, W. Van Roy, V. F. Motsnyi, M. Sawicki, G. Borghs, and J. De Boeck, Appl. Phys. Lett. **84**, 3495 (2004).

[6]J. Kreissl, W. Gehlhoff, and H. Vollmer, Phys. Rev. B **49**, 10307 (1994); J. Martin, J. Wedekind, H. Vollmer, and R. Labusch, *ibid.* **61**, 1918 (2000).

[7]T. Dietl, H. Ohno, and F. Mutsukura, Phys. Rev. B **63**, 195205 (2001).

[8]U. Gottlieb, A. Sulpice, B. Lambert-Andron, and O. Laborde, Alloys Comp. **361**, 13 (2003); A. Sulpice, U. Gottlieb, M. Affronte, and O. Laborde, J. Magn. Magn. Mater. **272–276**, 519 (2004).

[9]D. B. Migas, V. L. Shaposhnikov, A. B. Filinov, V. E. Borisenko, and N. N. Dorozhkin, Phys. Rev. B **77**, 075205 (2008); Y. Miyazaki, D. Igarashi, K. Hayashi, T. Kajitani, and K. Yubuta, *ibid.* **78**, 214104 (2008).

[10]Minhyea Lee, Y. Onose, Y. Tokura, and N. P. Ong, Phys. Rev. B **75**, 172403 (2007); F. P. Mena, D. van der Marel, A. Damascelli, M. Fath, A. A. Menovsky, and J. A. Mydosh, *ibid.* **67**, 241101(R) (2003).

[11]M. Bolduc, C. Awo-Affouda, A. Stollenwerk, M. B. Huang, F. G. Ramos, G. Agnello, and V. P. LaBella, Phys. Rev. B **71**, 033302 (2005).

[12]T. Dubroca, J. Hack, R. E. Hummel, and A. Angerhofer, Appl. Phys. Lett. **88**, 182504 (2006).

[13]A. F. Orlov, A. B. Granovsky, L. A. Balagurov, I. V. Kulemanov, Yu. N. Parkhomenko, N. S. Perov, E. A. Gan'shina, V. T. Bublik, K. D. Shcherbachev, A. V. Kartavykh, V. I. Vdovin, A. Sapelkin, V. V. Saraikinf, Yu. A. Agafonov, V. I. Zinenko, A. Rogalev, and A. Smekhova, JETP **109**, 602 (2009).

[14]A. Wolska, K. Lawniczak-Jablonska, M. Klepka, and M. S. Walczak, Phys. Rev. B **75**, 113201 (2007).

[15]S. Zhou, K. Potzger, G. Zhang, A. Mucklich, F. Eichhorn, N. Schell, R. Grotzschel, B. Schmidt, W. Skorupa, M. Helm, and J. Fassbender, Phys. Rev. B **75**, 085203 (2007).

[16]V. Ko, K. L. Teo, T. Liew, T. C. Chong, M. MacKenzie, I. MacLaren, and J. N. Chapman, J. Appl. Phys. **104**, 033912 (2008).

[17]Q. Liu, W. Yan, H. Wei, Z. Sun, Z. Pan, A. V. Soldatov, C. Mai, C. Pei, X. Zhang, Y. Jiang, and S. Wei, Phys. Rev. B **77**, 245211 (2008).

[18]S. Zhou, A. Shalimov, K. Potzger, M. Helm, A. Fassbender, and H. Schmidt, Phys. Rev. B **80**, 174423 (2009).

[19]X. C. Liu, Z. H. Lu, Z. L. Lu, L. Y. Lv, X. S. Wu, F. M. Zhang, and Y. W. Du, J. Appl. Phys. **100**, 073903 (2006); X. C. Liu, Y. B. Lin, J. F. Wang, Z. H. Lu, Z. L. Lu, J. P. Xu, L. Y. Lv, F. M. Zhang, and Y. W. Du, *ibid.* **102**, 033902 (2007).

[20]S. H. Chiu, H. S. Hsu, and J. C. A. Huang, J. Appl. Phys. **103**, 07D110 (2008).

[21]L. Zeng, E. Helgren, M. Rahimi, F. Hellman, R. Islam, B. J. Wilkens, R. J. Culbertson, and D. J. Smith, Phys. Rev. B **77**, 073306 (2008).

[22]V. V. Rylkov, B. A. Aronzon, Yu. A. Danilov, Yu. N. Drozdov, V. P. Lesnikov, K. I. Maslakov, and V. V. Podol'skii, JETP **100**, 742 (2005).

[23]S. N. Nikolaev, B. A. Aronzon, V. V. Ryl'kov, V. V. Tugushev, E. S. Demidov, S. A. Levchuk, V. P. Lesnikov, V. V. Podol'skii, and R. R. Gareev, JETP Lett. **89**, 603 (2009).

[24]J.-H. Yao, S.-C. Li, M.-D. Lan, and T.-S. Chin, Appl. Phys. Lett. **94**, 072507 (2009).

[25]E. S. Demidov, Yu. A. Danilov, V. V. Podol'skii, V. P. Lesnikov, M. V. Sapozhnikov, and A. I. Suchkov, JETP Lett. **83**, 568 (2006).

[26]P. E. Dyer, R. D. Greenough, A. Issa, and P. H. Key, Appl. Phys. Lett. **53**, 534 (1988); D. R. Ermer, S. C. Langford, and J. T. Dickinson, **81**, 1495 (1997).

[27]A. Lomov (private communication).

[28]*Handbook of Physical Quantities*, edited by I. S. Grigoriev and E. Z. Meilikhov (CRC Press, Boca Raton, FL, 1995).

[29]F. Matsukura, M. Sawicki, T. Dietl, D. Chiba, and H. Ohno, Physica E **21**, 1032 (2004).

[30]T. Fukumura, H. Toyosaki, K. Ueno, M. Nakano, T. Yamasaki, and M. Kawasaki, Jpn. J. Appl. Phys. **46**, L642 (2007); N. Nagaosa, J. Sinova, S. Onoda, A. H. MacDonald, and N. P. Ong, Rev. Mod. Phys. **82**, 1539 (2010).

[31]V. N. Men'shov, V. V. Tugushev, and S. Caprara, Eur. Phys. J. B **77**, 337 (2010); V. N. Men'shov, V. V. Tugushev, S. Caprara, and E. V. Chulkov, Phys. Rev. B **83**, 035201 (2011).

[32]A. P. Levanyuk, V. V. Osipov, A. S. Sigov, and A. A. Sobyanin, Zh. Eksp. Teor. Fiz. **76**, 345 (1979) [Sov. Phys. JETP **49**, 176 (1979)].

[33]T. Moriya, *Spin Fluctuation in Itinerant Electron Magnetism* (Springer, Berlin, 1985).

[34]K. K. Murata and S. Doniach, Phys. Rev. Lett. **29**, 285 (1972).

[35]T. Jungwirth, K. Y. Wang, J. Mašek, K. W. Edmonds, J. König, J. Sinova, M. Polini, N. A. Goncharuk, A. H. MacDonald, M. Sawicki, A. W. Rushforth, R. P. Campion, L. X. Zhao, C. T. Foxon, and B. L. Gallagher, Phys. Rev. B **72**, 165204 (2005).

[36]C. Timm, J. Phys.: Condens. Matter **15**, R1865 (2003).

[37]D. J. Priour Jr., E. H. Hwang, and S. Das Sarma, Phys. Rev. Lett. **92**, 117201 (2004).

[38]C. P. Moca, B. L. Sheu, N. Samarth, P. Schiffer, B. Janko, and G. Zarand, Phys. Rev. Lett. **102**, 137203 (2009).